ELSEVIER

Surface Science 471 (2001) 71–79

SURFACE SCIENCE

www.elsevier.nl/locate/susc

Amplitude, deformation and phase shift in amplitude modulation atomic force microscopy: a numerical study for compliant materials

Alvaro San Paulo, Ricardo García *

Instituto de Microelectrónica de Madrid, CSIC, Isaac Newton 8, 28760 Tres Cantos, Madrid, Spain

Received 29 April 2000; accepted for publication 26 September 2000

Abstract

Numerical simulations were applied to investigate the motion of a tip interacting with a compliant sample. The dependence of the amplitude, deformation, contact time and phase shift on the mechanical properties of the sample, free oscillation amplitude and cantilever force constant were investigated. The compliance and surface adhesion energy favour the formation of an adhesion neck between tip and surface. The neck modifies the tip motion when its length is comparable to the free oscillation amplitude. The simulations also show that the tip may oscillate fully indented on the sample if large force constant cantilevers and amplitudes are used. A good compromise between stability and resolution is achieved by using low force constant cantilevers and large oscillation amplitudes. The agreement obtained between theory and experimental data supports the conclusions of the model.

Keywords: Atomic force microscopy; Computer simulations; Energy dissipation; Adhesion

1. Introduction

Dynamic atomic force microscopy (AFM) is emerging as one of the dominant techniques for atomic and nanometer-scale characterization of surfaces. High resolution images of DNA [1], proteins [2,3] and several polymers have been obtained in air and liquids, as well as *true* atomic resolution images of several semiconductor [4,5] and inorganic surfaces [6]. The amplitude modulation method, also called tapping-mode AFM, is the method of choice when the experiments are performed in air or liquids.

Recently several contributions have been devoted to explain the dynamics of an oscillating tip in the amplitude modulation mode [7–20]. Amplitude modulation experiments usually involve amplitudes in the 5–100 nm range. The theoretical analysis of large amplitude oscillations is complicated by several factors. The force gradient varies considerably during an oscillation. This introduces nonlinear features in the dynamics of the tip motion. It also compromises the use of harmonic approximations [21]. Furthermore dissipative processes such as surface adhesion hysteresis, viscoelasticity or electronic dissipation may also be involved [22,23]. As a consequence, most of the

* Corresponding author. Fax: +34-91-806-0701.
E-mail address: rgarcia@imm.cnm.csic.es (R. García).

0039-6028/01/$ - see front matter
PII: S0039-6028(00)00883-9

theoretical descriptions have made use of numerical simulations. Those simulations were performed for materials with Young's modulus of several GPa. It was assumed that the results could be extrapolated to materials with smaller Young's modulus with minor corrections to account for the sample deformation.

In this paper numerical simulations are applied to study amplitude modulation experiments on compliant materials. A compliant material is loosely defined here as a material with a Young's modulus ranging between 1 and 100 MPa. The upper limit is introduced to avoid the presence of more than one steady state oscillation [24]. The lower limit is imposed by the geometry of the tip and the approximation used to calculate long-range attractive forces.

The model is applied to simulate the experiments performed by Bar et al. on polydimethylsiloxane (PDMS) by tapping-mode AFM [25,26]. The simulations reproduce the observed dependence of the amplitude and phase shift curves on the distance. The quantitative agreement between simulations and experiments can be interpreted as the suitability of the model to predict and understand the experimental data.

In Sections 2 and 3 the model and the computational method are described. Amplitude, average force, contact time and deformation dependencies on tip–sample separation, material and cantilever properties are analysed in Section 4. The comparison between experimental and simulated data is discussed in Section 5. Finally, in Section 6 our main findings and their experimental implications are summarized.

2. Model

The cantilever-tip motion in dynamic AFM is approximately described by the second-order differential equation

$$m\ddot{z} = -k_c z - \frac{m\omega_0}{Q}\dot{z} + F_{ts} + F_0\cos\omega t \qquad (1)$$

The contributions in the right hand side of the above equation are the elastic response of the cantilever, the hydrodynamic damping with the medium, the tip–surface interaction F_{ts}, that includes conservative and dissipative forces, and the excitation force $F_0\cos\omega t$. Q, $\omega_0 = 2\pi f_0$ and k_c are the quality factor, angular resonance frequency and spring constant of the free cantilever, respectively. The above equation implies several assumptions. (i) It considers the cantilever-tip ensemble as a point-mass spring. (ii) The Q-factor used here is independent of tip–sample separation. The first assumption ignores the contribution to the cantilever motion of the higher flexural modes of the lever [27]. The second assumption neglects changes in the hydrodynamic damping of the cantilever during its motion [28].

The tip–sample geometry is simulated by a sphere (tip) and a flat (sample). The conservative tip–sample interaction contains attractive and repulsive conservative forces. Long range attractive forces are derived from the nonretarded van der Waals energy for two atoms in vacuum. Assuming additivity, for a sphere–flat geometry the van der Waals force is

$$F_{vdw} = -\frac{HR}{6(z+z_c)^2}, \quad d \geqslant a_0 \qquad (2)$$

where H is the Hamaker constant and R the tip radius. For convenience, the tip–sample instantaneous separation d is calculated as the sum of the tip–sample rest distance (z_c) and the instantaneous tip position z ($d = z_c + z$). The origin of the z coordinate is the tip's rest position (Fig. 1). a_0 is an intermolecular distance that is introduced to

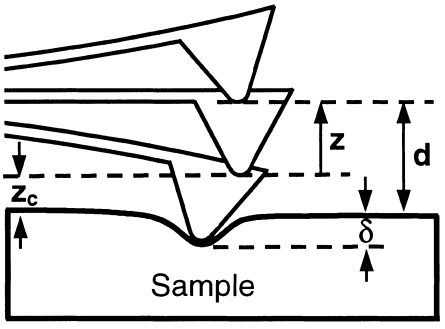

Fig. 1. Scheme of the cantilever-tip and the sample. The average (rest) cantilever position is the origin of the z coordinate. The instantaneous tip–sample separation d is the sum of the rest separation z_c (positive) and z (with its sign).

avoid the divergence of Eq. (2). For separations $d < a_0$, the resulting van der Waals force is identified with the force given by the Johnson–Kendall–Roberts model (JKR) [29] for $d = 0$:

$$\frac{8}{9}F_a = \frac{8}{3}\pi R\gamma = \frac{HR}{6a_0^2} \tag{3}$$

In addition to the adhesion force, during the contact ($d < a_0$) there are repulsive forces arising from Pauli and ionic repulsion. The repulsive force and the sample deformation are modelled by using JKR contact mechanics. This model allows to express the penetration as a function of the applied force,

$$\overline{\delta} = 3\left(\overline{F_{JKR}} + 2 + 2\sqrt{1+\overline{F_{JKR}}}\right)^{2/3} - 4\left(\overline{F_{JKR}} + 2 + 2\sqrt{1+\overline{F_{JKR}}}\right)^{1/6} \tag{4}$$

where $\overline{\delta} = \delta/\delta_a$ and $\overline{F_{JKR}} = F_{JKR}/F_a$ are the normalized penetration (indentation) and force respectively.

The adhesion force F_a is given by Eq. (3) while the pull-off separation or the length of the adhesion neck is calculated by

$$\delta_a = \left(\frac{\pi^2 R\gamma^2}{3\overline{E}^2}\right)^{1/3} \tag{5}$$

where $1/\overline{E} = (3/4)((1-\nu_t^2)/E_t + (1-\nu_s^2)/E_s)$ is the effective elastic modulus of the interface. When tip and sample are in mechanical contact the force is given by F_{JKR}.

The JKR model has been chosen because the elasticity parameter of the materials simulated here are $\lambda = 13$, 6 and 3 for 1, 10 and 100 MPa respectively (see Ref. [30] for a discussion about the use of contact mechanics models in scanning probe microscopy). The JKR model may not be suitable to explain some phenomena involving characteristic lateral scales below 1 nm, where the discrete character of the matter cannot be ignored. However, this limitation does not seem to have practical consequences for the cases considered here (see below). On the other hand, the JKR model assumes an elastic response in the quasistatic limit while the simulations presented here involve dynamic processes in the μs range. Previous theory–experiment comparisons [3,9,22,24] seem to support the use of quasistatic contact mechanics models in this context.

In the simulations the tip experiences a succession of loading–unloading cycles. Upon contact the JKR model allows the deformation of the sample and the formation of a neck. As a consequence a hysteresis appear in the force curve. It is assumed that elastic waves are generated during the rupture of the neck.

Compliant samples may involve several inelastic or dissipative processes. Friction, adhesion energy hysteresis or various plastic deformations have been invoked in different AFM experiments. In the absence of lateral displacements the energy dissipated by the frictional force existing between the tip and the sample can be considered negligible. Quantitative models to determine the adhesion energy hysteresis as a function of the material properties are still under development. As a consequence we limit the dissipative processes in the sample to the viscoelastic response of the material. In the Voigt model, the sample stress σ and the strain ε are related by

$$\sigma = G\varepsilon + \eta\frac{d\varepsilon}{dt} \tag{6}$$

Assuming that the viscous force has a relationship between contact area and sample deformation similar to the one given by the Hertz model, then

$$F_{vis} = -\eta\sqrt{R\delta}\frac{d\delta}{dt} \tag{7}$$

3. Numerical simulations

In the model the sample is characterized by the Young modulus E, the Hamaker constant H, the surface energy γ and the Poisson coefficient ν. The comparison between experiments and simulations have been performed for PDMS $E = 2$ MPa, $\gamma = 10$ mJ/m^2, $\nu = 0.45$ and $\eta = 5$ Pa s. The Hamaker values are deduced from the Lifshitz theory, $H = 2\times10^{-20}$ J. For the cantilever-tip system we have used a radius $R = 15$ nm, $Q = 400$, $f_0 = 160$ kHz and $k_c = 30$ N/m, unless otherwise stated.

Most of the cantilevers used in tapping-mode AFM are made of silicon with $E \approx 130$ GPa, i.e. several times higher than the E of the samples simulated here. We will assume that the total tip–sample force is relaxed in the deformation of the sample. The simulations have been performed for $f = f_0$.

A standard fourth-order Runge–Kutta algorithm has been used to solve Eq. (1). For each rest tip–sample separation, the conditions used to begin the numerical integration correspond to the preceding separation. The phase shift is extracted from the argument of the complex fast Fourier transform of the solution. The simulations show that in the cases studied here, the solution is well described by $z = z_0 + A\cos(\omega t - \Phi)$. The average force experienced by the tip during an oscillation is calculated by

$$\langle F_{\mathrm{ts}} \rangle = \frac{1}{T} \oint F_{\mathrm{ts}}(z(t))\,\mathrm{d}t \tag{8}$$

4. Amplitude, contact time and deformation

4.1. High force constant cantilevers and large amplitudes ($A_0 = 60$ nm)

Fig. 2(a) shows the oscillation amplitude dependence on the rest separation z_c for three different materials, $E = 1$, 10 and 100 MPa respectively. Three regions can be identified. For z_c values larger than the free amplitude, the amplitude is independent of the separation. Then there is a region where the amplitude decreases with z_c decreasing. At a separation that depends on the Young's modulus of the sample, an inflexion in the curve is observed. From there on the amplitude shows a slow dependence on the separation. In the intermediate region the slope increases with the stiffness of the sample. The curve for $E = 1$ MPa also shows a small but sharp drop from 60 to 58 nm. The solution of Eq. (1) for compliant materials give a single steady-state oscillation. This is in sharp contrast with the behaviour observed for stiff materials where a bi-stable oscillation has been described [24].

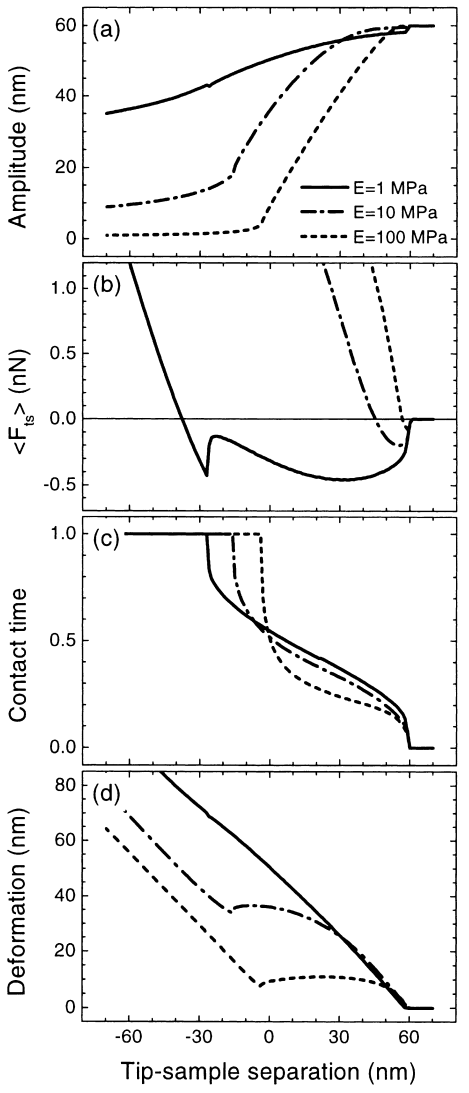

Fig. 2. (a) Amplitude, (b) average force, (c) contact time and (d) deformation dependence on tip–sample separation for three materials. $A_0 = 60$ nm, $R = 10$ nm, $k = 40$ N/m, $f_0 = 350$ kHz, $\gamma = 20$ mJ/m^2 and $\eta = 1$ Pa s.

The average forces experienced by the tip in a cycle are plotted in Fig. 2(b). The interval of z_c values where the average force is attractive decreases with E increasing. It involves an interval of 100 nm for $E = 1$ MPa while for $E = 100$ MPa is reduced to $\sim$4 nm. For the three materials, a small kink in the average force is observed.

To clarify the participation of short-range repulsive forces in the amplitude reduction, we have calculated the time per oscillation that the tip is in mechanical contact with the sample, t_c. Independent of the material elasticity, the curves show two sharp transitions. At $z_c = 60$ nm the contact time experiences a sudden change. The value of this change decreases with E. Decreasing the separation increases the contact time. Then another sharp change is observed. Its value increases with the Young's modulus. It also appears first for the stiffer material. The first change involves a transition from noncontact to a small but finite value of the contact time. The second change reflects the transition from a value of the contact time that is a fraction of the oscillation period to an oscillation where the tip is fully indented in the sample.

The comparison of Fig. 2(b) and (c) allows to associate the sharp minimum observed in the average force curve ($E = 1$ MPa) with the transition to an oscillation fully indented in the sample. An important observation concerning compliant materials and the use of large force constant cantilevers is that any given amplitude reduction involves tip–sample mechanical contact. This happens also in the cases where the average force is attractive.

The compliance of the sample is further revealed by calculating the tip's indentation or sample deformation δ as a function of the separation (Fig. 2(d)). The sample deformation or tip's indentation shows two regions. The first corresponds to oscillations with $t_c < T$ and the second to oscillations with $t_c = T$. The indentation increases with z_c and E^{-1} decreasing as could have been predicted. For $E = 1$ and 10 MPa there is a significant range of amplitudes where the tip oscillates fully indented in the sample. On the other hand, for $E = 100$ MPa the indentation at $t_c = T$ just reflects the cantilever deflection. Note that for $E = 1$ MPa an amplitude of $A = 0.8A_0$ implies a sample deformation of about 50 nm.

4.2. High force constant cantilevers and small amplitudes ($A_0 = 20$ nm)

Operating the microscope with smaller free oscillation amplitudes reduces the average force, however, the sample deformation is still considerable. The amplitude dependence on z_c is shown in Fig. 3(a). A local minimum is observed in the amplitude curves, especially for $E = 1$ MPa. The minimum gives rise to the existence of several separations that are compatible with the same amplitude. It also gives rise to negative differential amplitude regions. Those regions are not compatible with the standard logic used in the operation of the microscope. That logic assumes that the amplitude is reduced by approaching the tip towards the surface.

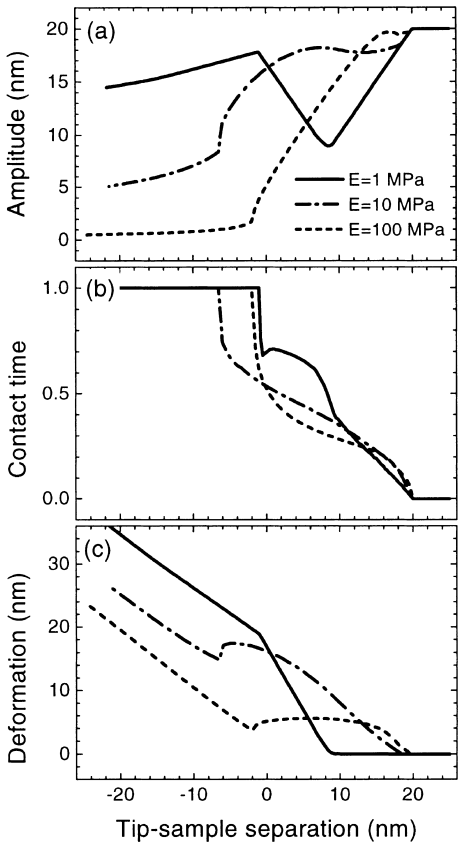

Fig. 3. (a) Amplitude, (b) contact time and (c) deformation dependence on tip–sample separation. $A_0 = 20$ nm, $R = 10$ nm, $k = 40$ N/m, $f_0 = 350$ kHz, $\gamma = 20$ mJ/m^2 and $\eta = 1$ Pa s.

The above minimum can be traced back to the formation and rupture of an adhesion neck when the tip is in mechanical contact with the sample a fraction of the period. This may perturb considerably the tip motion (Fig. 3(b)). This effect becomes noticeable when the length of the adhesion

neck is comparable to the free oscillation amplitude. The length of the neck is given by Eq. (5). It amounts 17, 4 and 1 nm for $E = 1$, 10 and 100 MPa respectively. The effect of the neck disappears once the tip oscillates fully indented in the sample because in this case there is not rupture of the neck. In fact some recent data reported Fain et al. [31] may support the formation of adhesive necks.

The use of a relatively small free oscillation amplitude $A_0 = 20$ nm still imply sample deformations of several nm (Fig. 3(c)). Notice that the existence of an adhesion neck is always associated with a finite contact time although it may be accompanied with a negligible sample indentation. This effect can be observed for $E = 1$ MPa and an interval of sample separations between 9 and 20 nm.

4.3. Low force constant cantilevers, $k = 1$ N/m

The use of low force constant cantilevers and large free oscillation amplitudes may provide an effective way to minimize the tip indentation in the sample. Fig. 4 shows the amplitude, contact time and deformation dependence on tip–sample separation. Although the amplitude reduction involves tip–sample mechanical contact, the contact time is rather small, about 3% of the period. Long-range attractive interactions control the tip motion without negligible sample deformation. In those cases, the average force is quite small (below 0.2 nN) and independent of E.

On the other hand, the combined use of small free oscillation amplitudes and low force cantilevers is discouraged. The amplitude curve for $A_0 = 10$ nm shows a hysteresis loop (Fig. 5(a)) when an approaching/retracting curve is calculated. This loop is caused by the formation of the adhesion neck upon tip–surface contact. The length of the adhesion neck is proportional to $E^{-2/3}$ which makes compliant materials more sensitive this effect. When the maximum kinetic energy of the tip is comparable to the energy dissipated in the formation and rupture of the adhesion neck, the tip is likely to be trapped by the neck. The trapping of the tip by the adhesion neck (see Fig. 5(b)) may damp considerably the tip oscillation for very compliant materials.

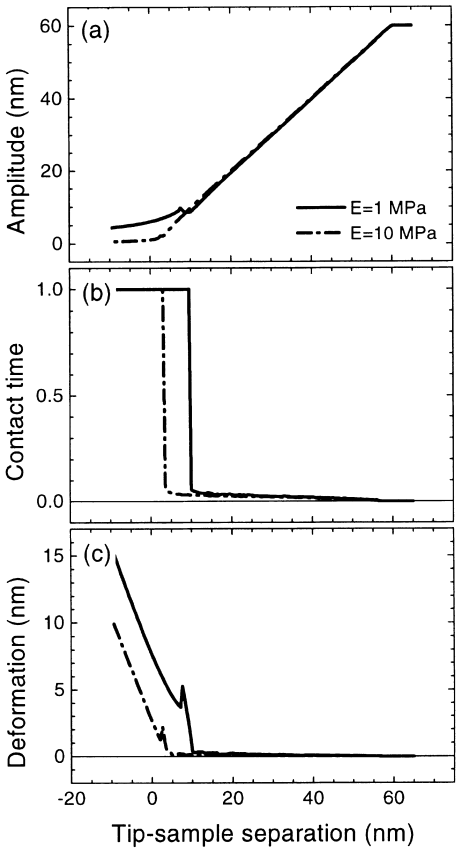

Fig. 4. (a) Amplitude, (b) contact time and (c) deformation dependence on tip–sample separation for a cantilever of $k = 1$ N/m and $f_0 = 100$ kHz, $A_0 = 60$ nm.

5. Comparison between theory and experiment

Theory and experimental data [25] for amplitude, phase shift, and average dissipated power are plotted in Fig. 6. The theory (solid line) reproduces the experimental data (open symbols). The experimental data corresponds to the sample labelled as "12" in Ref. [25]. The inflexion point observed at $z_c = -20$ nm in the theory (Fig. 6(a)) marks the transition to an oscillation where the tip is in mechanical contact with the sample during the whole cycle.

Phase contrast imaging in amplitude modulation AFM has been linked to tip–sample inelastic interactions. Based on the balance of energy sup-

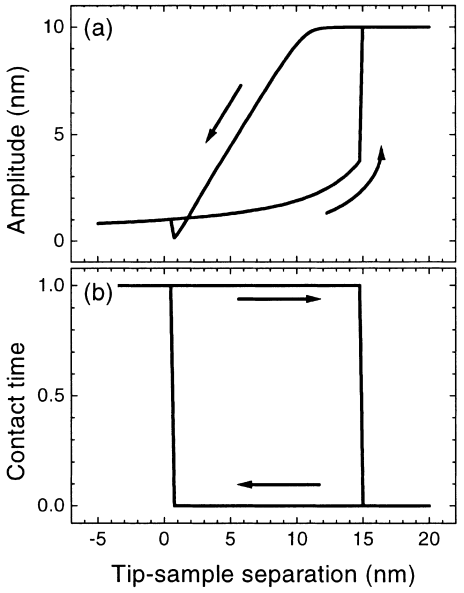

Fig. 5. (a) Amplitude, (b) contact time dependence on tip–sample separation for a cantilever of $k = 1$ N/m and $f_0 = 100$ kHz, $A_0 = 10$ nm, $E = 1$ MPa.

plied and dissipated by the cantilever Cleveland et al. [32] proposed the following

$$P_{\mathrm{ts}} = \frac{1}{2}\frac{kA^2\omega}{Q}\left(\frac{QA_0\sin\phi}{A} - \frac{\omega}{\omega_0}\right) \tag{9}$$

to turn the data of Fig. 6(b) into maps of energy (power) dissipation.

In Fig. 6(c) the experimental results and simulations of the average power dissipated by the tip–sample interaction forces are plotted. The average power increases with decreasing z_c until a maximum is found at -12 nm. There is a remarkable agreement between theory and experiment for a z_c interval ranging from -22 to 60 nm. When the tip oscillates completely indented in the polymer, the model predicts the qualitative behaviour of the data, although some numerical differences are observed.

The observed maximum underlines the sample viscoelastic properties. It is a consequence of two competing factors. The viscous force depends on the deformation and on velocity. The deformation increases while the average velocity of the tip decreases the with z_c decreasing. The difference in the rates of those changes produces the maximum.

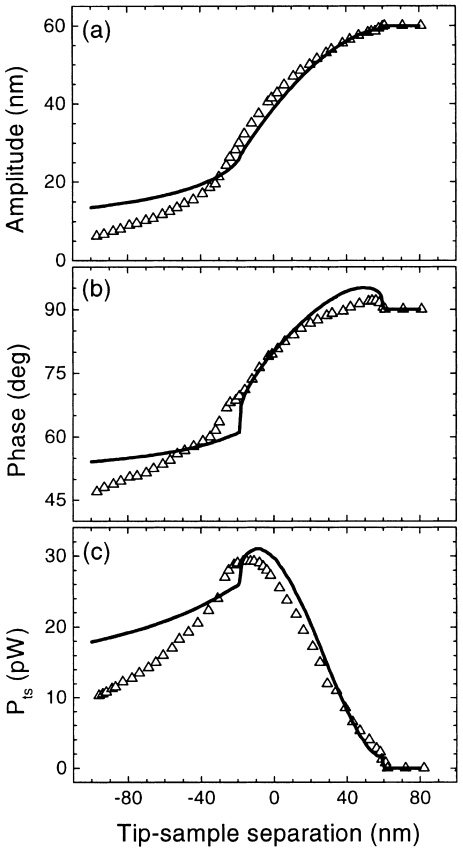

Fig. 6. (a) Amplitude, (b) phase shift and (c) average power dissipated in the sample dependence on the tip–sample separation. The open symbols correspond to the experimental data of Ref. [25] and the solid lines represent the simulations. $R = 15$ nm, $k = 30$ N/m, $f_0 = 160$ kHz, $E = 2$ MPa, $\gamma = 10$ mJ/m^2 and $\eta = 5$ Pa s.

Some numerical discrepancies are observed for indentations larger than the indentation corresponding to the inflexion point. Those are attributed to the tip shape. The model assumes a spherical tip-shape while the experiment involves a conical or pyramidal shape. For indentations $\delta \geqslant R$ the interaction force calculated here should differ from the experiment.

The ratio between the set point amplitude and the free oscillation amplitude $r_{\mathrm{sp}} = A/A_0$ is widely used as parameter to define the experimental operating conditions. In Fig. 7 the dependence of the

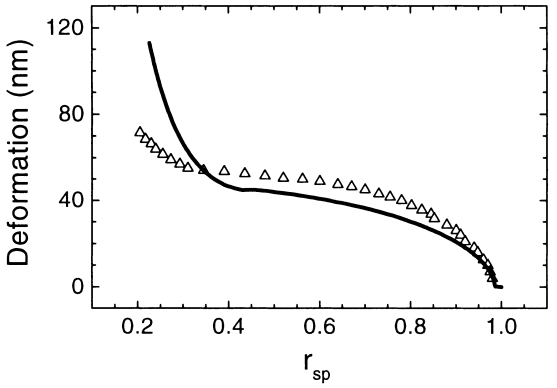

Fig. 7. Indentation depth as a function of the amplitude ratio. Theory (solid line) and experiments (open symbols). Parameters as in Fig. 6. Experimental data from Ref. [26].

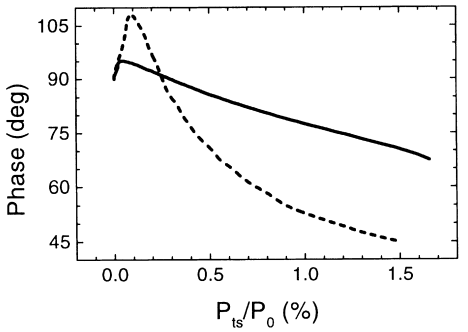

Fig. 8. Phase shift dependence on the reduced power dissipated by the sample. Parameters as in Fig. 6 for the solid line and $A_0 = 60$ nm, $R = 30$ nm, $k = 30$ N/m, $f_0 = 160$ kHz, $E = 10$ MPa, $\gamma = 20$ mJ/m^2 and $\eta = 5$ Pa s for the dashed line.

deformation $\delta \cong A_{sp} - z_c$ as a function of the set point amplitude is plotted. The data reveals that standard operating conditions (r_{sp} is usually in the range 0.4–0.8) involve substantial indentations in the sample although the average force remains small, below 1 nN. Again, there is a good agreement between experimental [26] (open symbols) and simulated data.

Bar et al. [25] have experimentally found for PDMS that the reduced tip–sample energy dissipation (P_{dis}/P_0, where P_0 is the total power of the tip motion) varies linearly with phase shift. From this observation, they have concluded that it is not the tip–sample energy dissipation but the reduced tip–sample energy dissipation that is relevant for the discussion of phase shift. To test the general character of the above result we have calculated the phase shift as a function of the reduced dissipated power for two different materials. For the set of values that reproduce the experimental data the simulations also show a linear relationship (Fig. 8, solid line). However, for a different material ($E = 10$ MPa) the phase shift shows a marked nonlinear behaviour (dashed line in Fig. 8). In fact, the nonlinear dependence between phase shift and the dissipated energy could have been anticipated by a close examination of Eq. (8).

6. Summary

We have presented a detailed analysis of the tip motion of a vibrating tip that interacts with a compliant material. The numerical study is focused on the amplitude, deformation, contact time and phase shift dependencies on the tip–surface separation. The results may be summarized in three points. First, the compliance of the material reduces the possible steady oscillations to one. Second, in most of the relevant experimental situations there is mechanical contact between tip and sample. Third, the formation of an adhesion neck upon mechanical contact is a relevant factor to determine the performance of the microscope.

The use of cantilevers with high force constants (above 10 N/m) and large free oscillation amplitudes (above 30 nm) produce sample deformations of several tens of nm. This observation has two implications. The lateral resolution is compromised. It cannot be better than the sample deformation. Second, large indentations may produce sample damage. A reasonable compromise between lateral resolution and stability may be achieved by using weak cantilevers $\sim$1–5 N/m and relatively large oscillation amplitudes $\sim$30–60 nm. Those conditions may imply an oscillation with negligible tip–surface mechanical contact. The good agreement between theory and experiment supports the conclusions and validates the general approach followed in this work.

The formation of an adhesion neck upon mechanical contact has relevant implications in the tip motion. It may produce regions of negative

differential amplitude. Those regions are incompatible with the standard operation of the AFM. On the other hand, if the length of the adhesion neck is comparable to the free oscillation amplitude the tip oscillation may be suppressed.

The energy dissipated by the tip–sample forces is relevant from the experimental point of view. It can be considered as an indirect estimation of the tip–sample damage. The competition existing between tip velocity and sample deformation produces a maximum in the dependence of P_{ts} as a function of the separation.

Acknowledgements

This work has been supported by the European Commission, BICEPS, BIO4-CT-2112 and Ministerio de Educación y Cultura (Spain), PB98-0471 A. San Paulo acknowledges financial support from the Comunidad Autónoma de Madrid.

References

[1] C. Bustamante, D. Keller, Phys. Today 48 (1995) 33.
[2] Möller, M. Allen, V. Elings, A. Engel, D. Müller, Biophys. J. 77 (1999) 1150.
[3] A. San Paulo, R. García, Biophys. J. 78 (2000) 1599.
[4] F.J. Giessibl, Science 267 (1995) 68.
[5] M. Guggisberg, M. Bammerlin, R. Lüthi, Ch. Loppacher, F. Battiston, A. Baratoff, E. Meyer, H.-J. Güntherodt, Appl. Phys. A 66 (1998) S245.
[6] F. Ohnesorge, Surf. Interf. Anal. 27 (1999) 379.
[7] B. Anczykowski, D. Krüger, H. Fuchs, Phys. Rev. B 53 (1996) 15485.
[8] B. Anczykowski, D. Krüger, K.L. Babcock, H. Fuchs, Ultramicroscopy 66 (1996) 51.
[9] R. García, A. San Paulo, Phys. Rev. B 60 (1999) 4961.
[10] R. García, A. San Paulo, Utramicroscopy 82 (2000) 79.
[11] J. Tamayo, R. García, Langmuir 12 (1996) 4430.
[12] A. Kühle, A.H. Soerensen, J. Bohr, J. Appl. Phys. 81 (1997) 6562.
[13] J.P. Hunt, D. Sarid, Appl. Phys. Lett. 72 (1998) 2969.
[14] L. Wang, Surf. Sci. 429 (1998) 178.
[15] G. Haugstad, R. Jones, Ultramicroscopy 76 (1999) 77.
[16] L. Nony, R. Boisgard, J.P. Aimé, J. Chem. Phys. 111 (1999) 1615.
[17] O.P. Behrend, L. Odoni, J.L. Loubet, N.A. Burnham, Appl. Phys. Lett. 75 (1999) 2551.
[18] M. Marth, D. Maier, R. Honerkamp, R. Brandsch, G. Bar, J. Appl. Phys. 85 (1999) 7030.
[19] G. Bar, L. Delineau, R. Brandsch, M. Ganter, M.-H. Whangbo, Surf. Sci. 457 (2000) L404.
[20] H. Bielefeldt, F. Giessibl, Surf. Sci. 440 (1999) L863.
[21] H. Hölscher, U.D. Schwarz, R. Wiesendanger, Appl. Surf. Sci. 140 (1999) 344.
[22] J. Tamayo, R. García, Appl. Phys. Lett. 71 (1997) 2394.
[23] B. Gotsmann, C. Seidel, B. Anczykowski, H. Fuchs, Phys. Rev. B 60 (1999) 11051.
[24] R. García, A. San Paulo, Phys. Rev. B 61 (2000) R13381.
[25] G. Bar, R. Brandsch, M. Bruch, L. Delineau, M.-H. Whangbo, Surf. Sci. Lett. 444 (2000) L11.
[26] G. Bar, L. Delineau, R. Brandsch, M. Bruch, M.-H. Whangbo, Appl. Phys. Lett. 75 (1999) 4198.
[27] U. Rabe, J. Turner, W. Arnold, Appl. Phys. A 66 (1998) S277.
[28] G. Chen, R. Warmack, A. Huang, T. Thundat, J. Appl. Phys. 78 (1995) 1464.
[29] K.L. Johnson, K. Kendall, A.D. Roberts, Proc. Roy. Soc. A 324 (1971) 301.
[30] W.N. Unertl, J. Vac. Sci. Technol. A 17 (1999) 1779.
[31] S.C. Fain, K.A. Barry, M.G. Bush, B. Pettiger, R.N. Louie, Appl. Phys. Lett. 76 (2000) 930.
[32] J.P. Cleveland, B. Anczykowski, A.E. Schmid, V.B. Elings, Appl. Phys. Lett. 72 (1998) 2613.